Roughness dependent wettability of sputtered copper thin films

Foadi, Farnaz; ten Brink, Gert H.; Mohammadizadeh, Mohammad Reza; Palasantzas, George

Published in:
Journal of Applied Physics

DOI:
10.1063/1.5092672

Journal of Applied Physics

Roughness dependent wettability of sputtered copper thin films: The effect of the local surface slope

Cite as: J. Appl. Phys. **125**, 244307 (2019); https://doi.org/10.1063/1.5092672
Submitted: 13 February 2019 . Accepted: 09 June 2019 . Published Online: 28 June 2019

Farnaz Foadi, Gert H. ten Brink, Mohammad Reza Mohammadizadeh, and George Palasantzas

Journal of Applied Physics ARTICLE scitation.org/journal/jap

Roughness dependent wettability of sputtered copper thin films: The effect of the local surface slope

Cite as: J. Appl. Phys. **125**, 244307 (2019); doi: 10.1063/1.5092672
Submitted: 13 February 2019 · Accepted: 9 June 2019 ·
Published Online: 28 June 2019

Farnaz Foadi,[1,2] Gert H. ten Brink,[2] Mohammad Reza Mohammadizadeh,[1] and George Palasantzas[2,a)]

AFFILIATIONS

[1]Supermaterials Research Laboratory (SRL), Department of Physics, University of Tehran, North Kargar Av., P.O. Box 14395-547, Tehran, Iran
[2]Zernike Institute for Advanced Materials, University of Groningen, Nijenborgh 4, 9747 AG Groningen, The Netherlands

[a)]**Author to whom correspondence should be addressed:** g.palasantzas@rug.nl

ABSTRACT

Here, we investigated the static and the dynamic wetting behaviors of copper (Cu) thin films deposited by DC magnetron sputtering. The deposited films have random rough surfaces for which the rms roughness amplitude σ, the lateral correlation length ξ, and the roughness exponent α were obtained from the analysis of height topography images acquired by atomic force microscopy. The time-dependent height-height correlation functions indicated anomalous kinetic roughening with roughness exponents $\alpha \approx 0.9$ and evolving roughness parameters σ and ξ with deposition time. The latter yields a nonstationary local surface slope σ/ξ that has a crucial impact on the surface wettability. Indeed, static and dynamic contact angles' (CAs) measurements revealed two wetting regimes associated with different growth stages leading to a transition from a metastable Cassie-Baxter to a Wenzel-like state for the roughest films. Moreover, the increasing roughness with well distributed peaks and valleys leads to increasing CAs due to trapped air in surface cavities, while after some point the larger surface features lead to a decrement of the CAs that vary only slightly with further roughening. Although the apparent wetting transition with increasing surface roughness is not favored by the local Laplace pressure estimation, the energy of the system decreases with surface roughening, or equivalently increasing local surface slope, favoring energetically a Wenzel state. Under these conditions, the water droplet can spontaneously fill the surface cavities once the impregnation is initiated by the hydrophilic nature of the surface, in agreement with our experiments for significantly large local surface slopes ρ (>0.1) and large roughness exponents $\alpha \sim 1$.

I. INTRODUCTION

Surface wetting has been studied extensively for more than 200 years because it has diverse applications in many fields as, for example, in anti-icing,[1] anticorrosion,[2] drag reduction,[3,4] water-repellency,[5,6] and medical sciences.[7,8] This surface property can be studied by a water sessile drop placed on a surface, where it reaches a stable state with lower energy. From the contact line between the droplet and the surface, the contact angle (CA) is derived. For smooth surfaces, the pioneering work was performed by Young,[9] where for a smooth and homogeneous surface, the apparent CA θ_y is given by the relation $\cos(\theta_y) = (\gamma_{sv} - \gamma_{sl})/\gamma_{lv}$ with γ_{sv}, γ_{sl}, and γ_{lv} being the solid-vapor, solid-liquid, and liquid-vapor surface tensions, respectively. However, most surfaces in nature and experiments are rough at various length scales. In order to incorporate the effect of roughness on the wettability of surfaces, two main models were proposed in the past by Wenzel[10] and Cassie and Baxter.[11] Indeed, Wenzel studied this effect theoretically assuming that the droplet wets the surface cavities beneath it. The CA is given in this case by the equation $\cos(\theta_w) = r\cos(\theta_y)$, where r is the roughness factor defined as the ratio of the actual surface area to the projected one. If a surface is hydrophilic in nature ($\theta_y < 90°$), then the roughness will make the surface more hydrophilic, while if a surface is hydrophobic ($\theta_y > 90°$), then the roughness will make it more hydrophobic. However, for rough surfaces, the water droplet does not necessarily penetrate all cavities leaving air pockets beneath the droplet. For this case, Cassie and Baxter[11] proposed the equation $\cos(\theta_{CB}) = f\cos(\theta_y) - (1 - f)$ to calculate the CA, where f (filling factor) is the fraction of the solid in contact with the droplet.

In this wetting state, the roughness increases the CA for both hydrophilic and hydrophobic surfaces.

Nowadays, it is well established that the control of surface wettability can be achieved by altering the surface chemical composition and/or surface roughness.[12–15] For different applications, both hydrophobic and hydrophilic coatings can be important. In some cases, hydrophobic surfaces will resemble the lotus effect,[16–19] producing water-repellent and self-cleaning surfaces due to the weak adhesion of water droplets. Another possibility is the rose petal effect,[20–22] which is characterized by the strong surface adhesion leading to pinning of water droplets and high contact angles. On the other hand, hydrophilic coatings can be made from metals and metal oxides.[23–26] In any case, many studies have been devoted to understand the effect of micrometer scale roughness either random or structured on the wetting behavior of surfaces.[27–30] Specifically, several efforts have been focused on producing fractal structures to achieve super-water-repellent or superhydrophobic surfaces.[31,32] Indeed, dual scale roughness (micrometer and nanometer scale roughness known as hierarchical roughness) favors superhydrophobicity.[33–36]

Furthermore, nanoscale random roughness has been shown theoretically to have a relationship to the statistical roughness parameters as the roughness exponent α ($0 < \alpha < 1$), which characterizes the degree of roughness irregularity at short length scales ($\ll\xi$, with ξ being the lateral correlation length), and the long wavelength roughness ratio σ/ξ with σ being the rms roughness amplitude (assuming weak surface roughness $\sigma/\xi \ll 1$).[37] Another numerical work showed the impact of the roughness exponent α and mean square surface slope in tuning surface hydrophobicity.[38] In another study for randomly rough surfaces, a threshold value for the Wenzel roughness parameter has been obtained for superhydrophobicity.[39] Besides other theoretical works on wetting,[40,41] several research efforts have been focused on the effect of statistical parameters on the wettability of thin films. For example, Yadav *et al.*[42] investigated the wettability of some fractal-structured surfaces, and it was concluded that higher fractal dimension leads to higher CAs. In another work,[43] the correlation between surface-roughness parameters and wetting was explored experimentally, indicating that the CA decreases with increasing local surface slope $\rho \propto \sigma/\xi^{\alpha}$. Patra *et al.*[44] modified the surface morphology by annealing, and they found increasing CAs with increasing surface roughness. On the other hand, Chatterjee *et al.*[45] have shown that the rms roughness σ and the correlation length ξ increase with deposition angle leading to higher CAs due to lower roughness exponents α and increased surface porosity.

So far, the effect of random roughness evolution during thin film growth on surface wettability remains only partially understood to enable control of this surface property toward emerging technology applications, where the control of hydrophobicity and hydrophilicity is necessary. In this respect, we considered here to study the wetting behavior of sputtered Cu thin films that are relevant in widespread technology applications such as inkjet printing technology, solar cells, integrated circuits, and heat transfer technology.[46–49] Particular attention was paid to wetting transition between metastable Cassie-Baxter (CB) and W states as a function of the evolving surface-roughness parameters by taking into account the energy of the system and the local Laplace pressure that controls wetting in surface cavities.

II. EXPERIMENTAL METHODS

Copper thin films were prepared using DC magnetron sputtering (Mantis Deposition Ltd.) on Si (100) substrates with native oxide (having rms roughness $\sigma < 2$ nm) at room temperature (see Fig. 1), which have typical measured CAs $\sim 32°$. The base system pressure was less than 10^{-7} mbar, while during deposition the sputtering pressure was 10^{-3} mbar (having a DC power of 63 W at 40 sccm of Ar 5.0 as sputtering gas). Sputtering took place from a high-purity Cu target (99.999%) at an angle of 30° and a distance of 20 cm with respect to the normal from the sample surface. In order to obtain films with different roughness, Cu deposition was performed from 30 min to 6 h (under identical conditions on different Si wafers from the same batch) yielding film thicknesses in the range ~60–750 nm with an average deposition rate of ~2 nm/min. The latter was evaluated using atomic force microscopy (AFM) at a step edge as it is shown in Fig. 2(a). It must be noted that during sputtering, Cu oxidation takes place in agreement with our former transmission electron microscopy (TEM) studies of Cu nanoparticles (NPs). The latter were prepared under similar Ar flows within the same chamber (having a separate sputter source designed to produce nanoparticles) in the absence of any reducing gas.[50] In any case, upon exposure to air, the formation of a thin layer of Cu oxide ~1–3 nm thick is unavoidable, and its surface energy will play a dominant role in the wetting process.[50]

Furthermore, the surface morphology of the Cu films was imaged by AFM (Bruker, Multimode 8) at ambient temperature operated in tapping™ mode using an AFM tip (NSC15/No Al from MikroMasch, USA) with a tip radius of 8 nm. The AFM topography images were taken over scan areas of $1 \times 1\,\mu m^2$ and $1.5 \times 1.5\,\mu m^2$, which are significantly larger than the Cu grain size, with a resolution of 1024×1024 pixels, at five different locations on each sample. High resolution images of the microstructure of the Cu surfaces were also obtained using a scanning electron microscope (SEM, FEI NovaNanoSEM 650) equipped with an in-lens [through the lens dectector (TLD)] secondary electron (SE) detector.

Finally, the wettability of the as-deposited Cu surfaces was studied measuring both static and dynamic CAs by the sessile-drop method on a Dataphysics OCA15 system coupled with a camera that could record pictures over several seconds. A $2\,\mu l$ pure water droplet (MiliQ) was gently dropped on the surface by an automated syringe at a rate of $0.5\,\mu l/s$. The measurement of the advancing CA was performed by increasing the volume of water to $8\,\mu l$ at a rate of $0.2\,\mu l/s$, while the receding CA was performed by removing water from the surface at a rate of $0.2\,\mu l/s$ by keeping the syringe into the droplet. In order to gauge the effect of surface hydrocarbons, an average of at least 10 measurements for the CAs was taken for each Cu sample in different days after preparation. The samples were stored in vacuum after preparation to minimize hydrocarbon adsorption prior to CA measurements and after completion of the measurements. Although the CA measurements were not performed at equal times after preparation (despite the vacuum storage) for the different samples, we repeated the CA measurements for several days after the first set of measurements (for a period of a week), and we observed no meaningful difference between the CA values. In addition, experiments that are more detailed were performed to investigate the wetting behavior of the Cu samples with respect to aging and

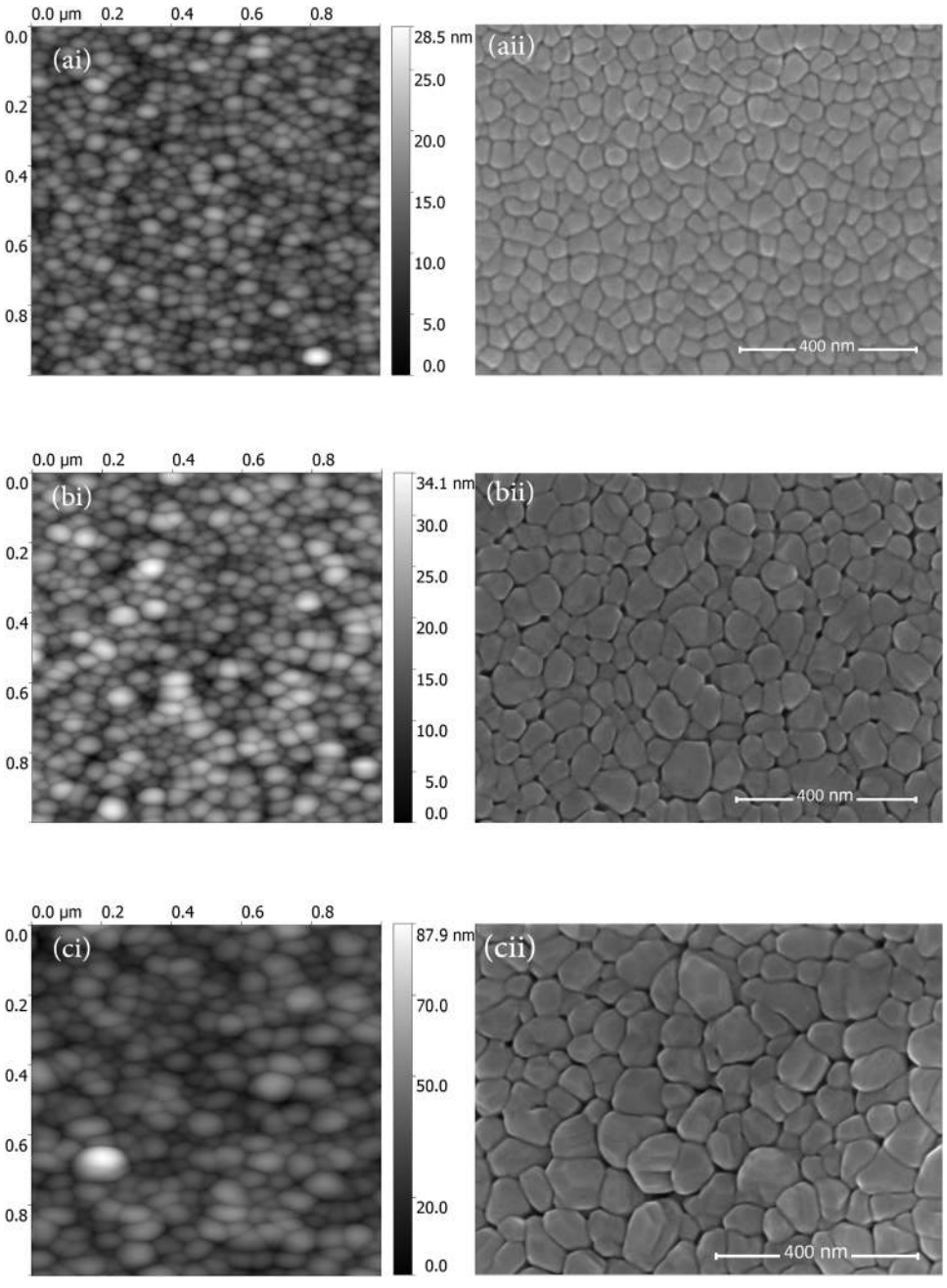

FIG. 1. Representative AFM (i) and SEM (ii) images of Cu surfaces for (a) 1 h, (b) 2 h, and (c) 6 h of Cu deposition.

associated hydrocarbon adsorption after exposure to ambient for almost one year.

III. KINETIC ROUGHENING OF SPUTTERED FILMS

Figure 1 shows AFM and SEM topography images of representative Cu surfaces. The scan sizes for the AFM images are more than 10 times larger than the lateral correlation length ξ in order to be statistically relevant. From the SEM images, the grain growth with deposition time is evident, while the AFM images show both the roughening and the coarsening processes during growth. Indeed, as it is shown in Fig. 2(b), the root mean square roughness $\sigma = \langle [h(x, y)^2]^{1/2} \rangle$, where $h(x, y)$ is the surface height at the position $\mathbf{r} = (x, y)$ around the mean value $\langle h(x, y) \rangle = 0$ (with $\langle \cdots \rangle$ an ensemble average), is increasing with film thickness or deposition time for fixed deposition rate. Similarly, the lateral correlation

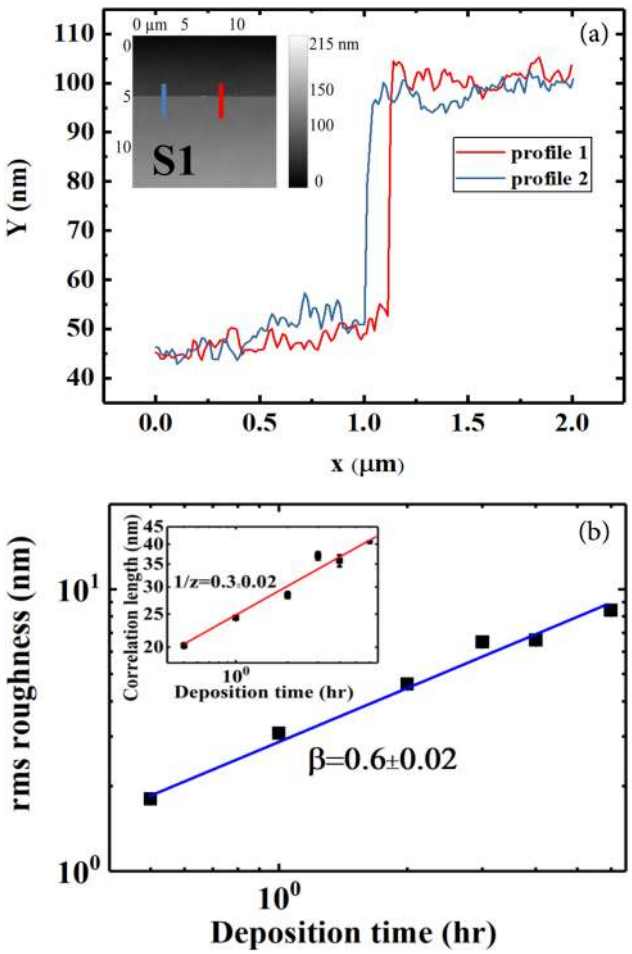

FIG. 2. (a) Height profiles of two different regions near the step for sample S1 accompanied by the AFM image as an inset. (b) The variation of the rms roughness amplitude σ and the correlation length ξ with the deposition time.

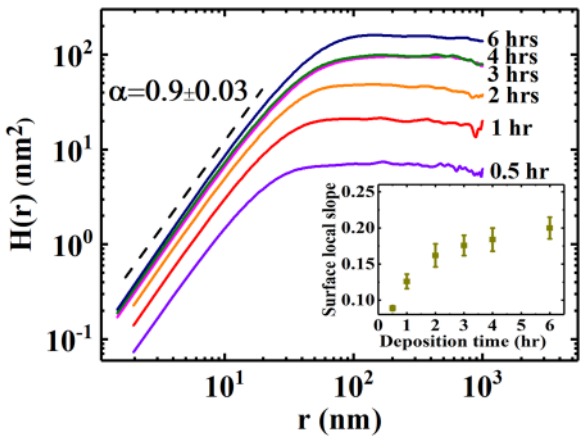

FIG. 3. Log-log plot of the time-dependent height-height correlation function for the different Cu films. As it is indicated by a dashed line, all the correlation curves scale the same at short length scales (<ξ) with slope 2α that yields the roughness exponent α = 0.9 ± 0.03. The inset shows the variation of the local slope ∼σ/ξ with the deposition time.

length ξ also increases with deposition time [the inset of Fig. 2(b)]. The measurement of the height-height correlation function $H(\mathbf{r}) = \langle[h(\mathbf{r}) - h(0)]^2\rangle$ (see Fig. 3) allows determination of all the statistical parameters, namely, the rms roughness amplitude σ, the roughness exponent α, and the lateral correlation length ξ because it follows the scaling behavior,[51,52]

$$H(\mathbf{r}) = \begin{cases} \propto \mathbf{r}^{2\alpha}, & r \ll \xi, \\ 2\sigma^2, & r \gg \xi. \end{cases} \quad (1)$$

The roughness exponent α ($0 < \alpha < 1$), for which lower values give more jagged surfaces at short length scales (<ξ), can be calculated from the linear fit of the log-log plot of the correlation function at $r < \xi$. The correlation length ξ can be determined from the intersection of the linear part with the saturation regime at $r \gg \xi$ that yields the value of the rms roughness amplitude σ. The roughness parameters for all Cu films are shown in Table I. The scan sizes for the AFM measurements were chosen sufficiently large ($\gg\xi$) to obtain the saturated rms roughness amplitude σ.[51–55]

The average roughness exponent for the Cu films was α = 0.9 ± 0.03. The log-log plots in Fig. 2 yield the growth exponent β = 0.6 ± 0.02 that describes the temporal evolution of the rms roughness amplitude $\sigma \propto t^{\beta}$ and the dynamic exponent $\frac{1}{z} = 0.3 \pm 0.02$ that describes the temporal evolution of the lateral correlation length $\xi \propto t^{\frac{1}{z}}$. The large value of α indicates surface diffusion as a surface relaxation mechanism during Cu deposition. However, since $\beta \neq \alpha/z$ the roughening of the growth front is anomalous with a time varying local surface slope.[53,54] This is also reflected by the plots of the height-height correlation at short length scales (<ξ) in Fig. 3, where the linear parts do not coincide, indicating that the average local surface slope $\rho = \langle(\nabla h)^2\rangle^{1/2} \propto \sigma/\xi^{\alpha}$ is not a time invariant of the roughening process. As a result, the relation $z = \alpha/\beta$ is no longer satisfied.[52,55] This is a sign of instability that leads to anomalous growth, as it has been observed in other metallic and nonmetallic films prepared by DC sputtering[56–58] where the angle between the substrate and the source beam leads to local shadowing effects. In any case, for more

TABLE I. Surface statistical parameters including the rms roughness amplitude σ, the correlation length ξ, and the roughness exponent α for the different Cu surfaces.

Sample	Scan size (μm^2)	σ (nm)	α	ξ (nm)
S1	1 × 1	1.8 ± 0.01	0.9 ± 0.02	20.2 ± 0.3
S2	1 × 1	3.08 ± 0.03	0.9 ± 0.03	24.4 ± 0.3
S3	1 × 1	4.6 ± 0.2	0.96	28.4 ± 0.6
S4	1.5 × 1.5	6.5 ± 0.2	0.94	37 ± 1
S5	1.5 × 1.5	6.6 ± 0.3	0.94	35.8 ± 1.4
S6	1.5 × 1.5	8.4 ± 0.2	0.96	41.4 ± 1.1

precise calculations, the average local surface slope ρ can be obtained by the analytic form[52]

$$\rho = \frac{\sigma}{\xi\sqrt{2}}\left(\frac{1}{1-\alpha}\left(\left[1+c(Q_c\xi)^2\right]^{1-\alpha}-1\right)-2c\right)^{1/2}, \qquad (2)$$

where $c = (1/2\alpha)(1-[1+c(Q_c\xi)^2]^{-\alpha})$ for $0<\alpha\leq 1$ and $Q_c = \pi/a_o$ with a_o being the lowest lateral roughness cutoff of atomic dimensions. For large roughness exponents $\alpha \sim 1$, as it is the case here for the sputtered Cu films, the average local surface slope can be approximated by the simple expression $\rho \approx \sigma/\xi$.

IV. SURFACE WETTING MEASUREMENTS

Figure 4 shows the variation of the static contact angle vs the deposition time for the Cu surfaces with the corresponding images of the water droplets. The static CA initially increases with the deposition time, while afterward it decreases and finally remains relatively constant for the thicker films. One gains more insight into the wetting behavior by the knowledge of the dynamic CAs, namely, the advancing (A) and the receding (R) CAs. The behavior of the A/RCAs with the deposition time is shown in Fig. 5. The contact angle hysteresis CAH (=ACA-RCA) shows almost the same variation with the deposition time as the static CA. The latter means that the ability of the Cu surfaces to advance the contact line does not change with the deposition time. This is because the RCA is relatively the same for all surfaces, while the difference between CA and ACA remains constant. As a result, the ACA can advance the droplet by the same magnitude.

From Fig. 5, it is evident that the RCA does not change significantly with deposition time and remains rather low RCA ~ 18° within the errorbar of the measurements. Nevertheless, our experimental observations indicated that the receding occurred at later times for the samples with higher rms roughness due to stronger

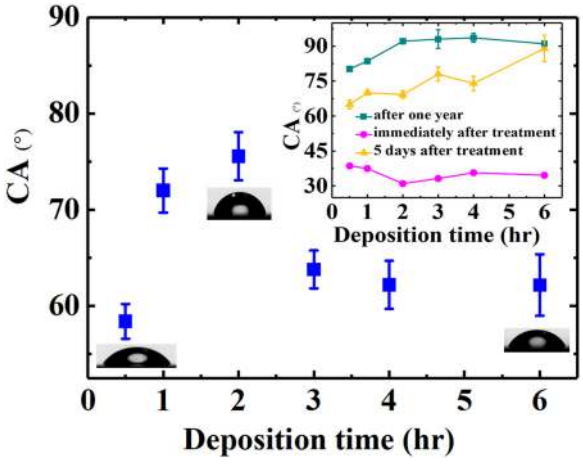

FIG. 4. CA vs deposition time for the various Cu thin films deposited with magnetron sputtering. The inset shows the CA behavior of the same Cu samples after 1 year, immediately after 30 min cleaning with UV-O_3 and 5 days after the UV-O_3 treatment.

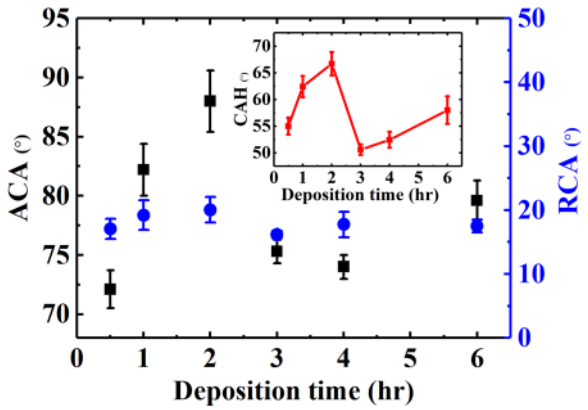

FIG. 5. The variation of ACA and RCA vs the deposition time. The inset shows the variation of the contact angle hysteresis (CAH = ACA-RCA) vs the deposition time.

pinning effects. The latter indicates significant temporal receding delay with increasing roughness. For example, the time difference at the onset of receding for sample S1 and sample S6 was ~4 s. Since the whole variation of CAH is ~50°–65°, the latter indicates that the water droplet tends to stick on the Cu-oxide surfaces indicating significant adhesion forces. Indeed, for low adhesion hydrophobic (e.g., lotus effect) and slippery surfaces, the CAH is less than 10°.

In order to understand the wettability of the Cu surfaces, we plotted in Fig. 6(a) the variation of CA with respect to the rms roughness amplitude σ and the correlation length ξ. The same trend is revealed as in Fig. 4, which displays the CA vs the deposition time. The latter shows that the roughness parameters σ and ξ play a crucial role in the magnitude of the CA. Since Cu-oxide (due to oxidation of Cu upon exposure to air) is a hydrophilic material, we can speculate that the first wetting regime is likely to be a metastable CB state that leads to increasing CA with increasing rms roughness (up to ~4.6 nm). Further roughening causes reduction of the CA with a W-like state to develop as a more dominant wetting state. The CAs obtained for the last three samples do not vary significantly, but they are still higher than for the first sample with the lowest rms roughness σ. The same behavior also develops for the CA variation with respect to the correlation length ξ. Furthermore, we plotted in Fig. 6(b) the variation of the CA with respect to the surface local slope ($\rho = \sigma/\xi$),[52,53] which is a measure of the long wavelength surface undulations. The CA is behaving in a similar manner as the main plot in Fig. 4. In any case, since the roughness exponent remains relatively constant during growth, it can be concluded that the rms roughness amplitude σ and the correlation length ξ play a dominant role on the CA as a function of the surface roughening.

Adsorbing hydrocarbons from the environment and its effect on the wetting behavior of surfaces have been addressed to a significant degree.[59–62] Therefore, it is noteworthy to investigate the wetting behavior of the prepared Cu films with the aging time and especially with respect to associated surface hydrocarbon adsorption. As a result after one year from synthesizing the Cu films,

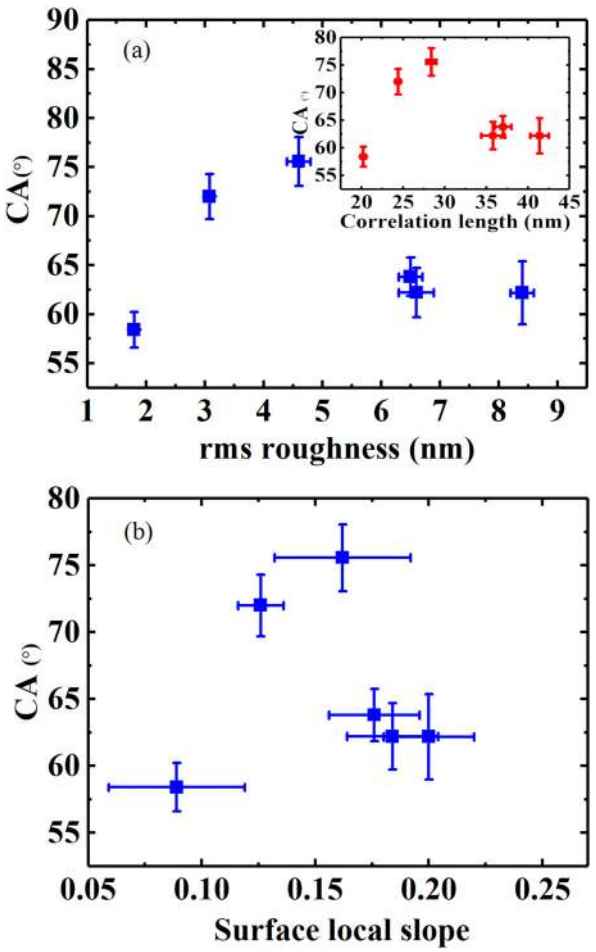

FIG. 6. The variation of CA with respect to the rms roughness σ (a) and surface local slope σ/ξ (b). The inset shows the variation of the CA with the correlation length ξ.

which were exposed to ambient conditions (air), we measured the static CA at different places on each surface. As it is shown in the inset of Fig. 4, the average values of the static CAs were higher than those that we measured a few days after Cu deposition (Fig. 4). This can be due to adsorption of hydrocarbons from the environment leading to higher CAs that usually takes place for noble metals like Cu. It can be seen that there is a decreasing trend for the thickest sample (e.g., sample S6), with an almost similar behavior as we obtained before for the as-deposited films in Fig. 4. In the next steps, we measured the CAs on all surfaces immediately after exposing them to UV-O_3 treatment for 30 min and after 5 days from this surface treatment. These measurements are shown in the inset of Fig. 4. The variation of the CAs immediately after the UV-O_3 treatment is ∼30°–40°, and these low angles are due to the removal of hydrocarbons leading to a very hydrophilic state that shows an overall W-like wetting behavior. We must note that the UV-O_3 surface treatment constitutes a separate study with respect to surface wetting, because this surface process could cause changes in the crystalline phase, leading to the appearance of new bonds.[63] As a result, the surface after UV-O_3 treatment is not the same as the as-deposited one, and it shows a highly hydrophilic wetting state (the inset of Fig. 4). In addition, the wetting behavior of the Cu surfaces after 5 days reveals their strong tendency to attract hydrocarbons leading to higher CAs. However, the CA now continues to increase also for the roughest films since hydrocarbons are adsorbed more intense now (after UV-O_3 treatment due to surface charges) in cavities that are increased in size with roughening leading to a CB-type wetting state. We should state here that the CA measurements for the thickest Cu film (sample S6) were performed at a longer time interval than that of the samples S4 and S5 (Fig. 4). The latter means that the low local slope plays a dominant role in obtaining lower CAs and observing a W-like state with increasing surface roughening after deposition.

Figure 7 shows representative surface height profiles and height distributions of all Cu surfaces. The different height profiles

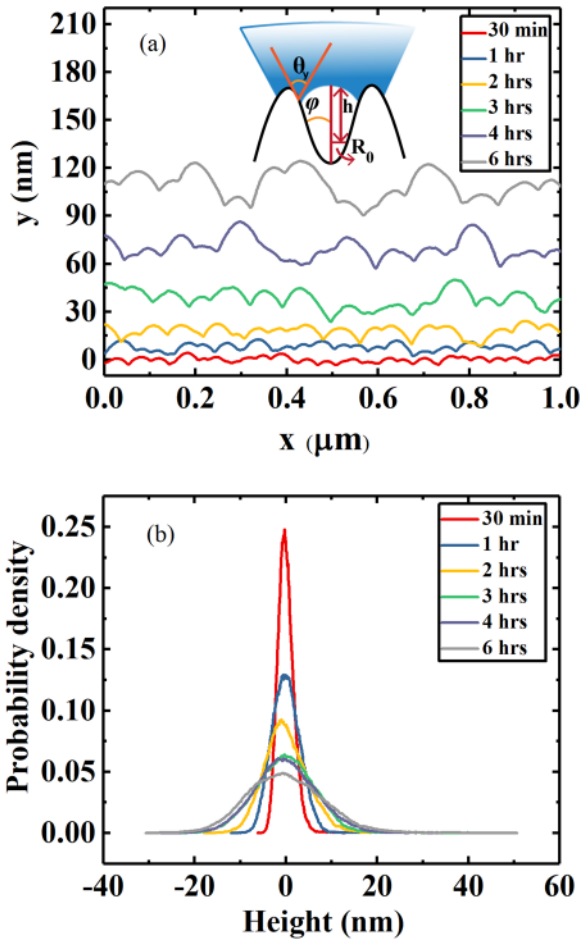

FIG. 7. (a) Surface height profiles and (b) height distributions of the Cu surfaces produced at different deposition times. The inset shows the shape of the local water meniscus on the cavities of the hydrophilic Cu surface.

of an AFM image for one sample were statistically the same. For sample S1, where we have the lowest CA, the number of high peaks on the surface is low. For sample S2, the number of high peaks as well as deep valleys increases. For sample S3, for which we obtained the highest CA, peaks with almost identical heights and deep valleys appear to dominate the surface profile. Finally, the samples S4, S5, and S6 show rather similar height profiles. Although one can observe high peaks and deep valleys, the CAs on these surfaces are lower, and the number of high peaks is less than in samples S2 and S3. At this point, it is important to obtain statistical feature related parameters of all the surfaces that can give more detailed information about the asymmetry and the shape of the corresponding surface profiles.

The surface skewness (Sk) and kurtosis (Ku) are the third and the fourth order moments of the height distribution function. Indeed, Sk describes the symmetry of the height distribution around the mean plane, and Ku is a criterion for the tailedness. The variation of CA with respect to Sk and Ku is shown in Fig. 8. All surfaces show positive skewness, which is the sign of peak dominance in agreement with the height profiles in Fig. 7(a). The sample S3 has the lowest Ku value, indicating that the distribution of the peaks and the valleys [Fig. 7(b)] is more centrally distributed around the mean plane with respect to the other samples. The latter can be verified from the height distribution in Fig. 7(b). From the height profiles and distributions in Fig. 7, we can infer that surfaces with well distributed high peaks and deep valleys favor increasing CAs with increasing surface roughness due to trapped air in surface cavities. However, after some point when larger surface features form (e.g., for the last three rougher surfaces), the CA decreases and varies slightly with further roughness evolution.

Furthermore, we will make an attempt to discuss the behavior of CA with respect to the CB-W transition that appears to take place with increasing surface roughness. Most of the research works have considered the effects of energy barriers and Laplace pressure for the CB-W transition in regular and pillarlike structures.[64–67] Only a few papers have studied these effects on random rough surfaces.[68,69] Here, we explore how the different parameters of a rough surface, namely, the rms roughness σ and the grain size (∼ξ), influence the energy and the Laplace pressure of a system, and consequently the CB-W transition. The energy barrier for this transition is known as the energy difference between the CB and the W states, which can be overcome by different factors such as water dropping from a height or changing the droplet volume,[70] droplet evaporation,[71] or by Laplace pressure.[65] For the 2 μl water droplet that we used in our experiments, assuming a spherical shape with a radius R = 0.78 mm, its weight could generate an inner Laplace pressure $P_g = 2\gamma_{lv}/R = 185$ Pa if we consider the water-air interfacial tension $\gamma_{lv} = 72$ mN/m.[72] The gravitational effect on the droplet is negligible because the droplet radius R is smaller than the capillary length[73] of water $l_g = \sqrt{(\gamma_{lv}/\rho g)} \sim 2.7$ mm with $g \sim 10$ m/s^2 and $\rho \sim 10^3$ kg/m^3. Therefore, due to the low pressure induced by the weight of the water droplet, there should be other local effects responsible for the CB-W transition.

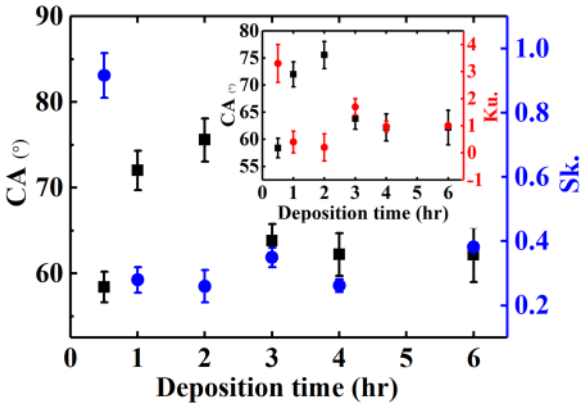

FIG. 8. The effect of skewness and kurtosis on the CA for the different Cu surfaces.

According to previous studies,[74] the Laplace pressure ΔP in a surface cavity depends on the local inclination angle of the surface feature, and it can be written as

$$\Delta P = P - P_0 = -\frac{\gamma_{lv} \cdot \cos(\theta_y - \varphi)}{R_0 + h \tan \varphi}. \quad (3)$$

In Eq. (3), P is the pressure in the liquid side of the meniscus touching the surface, P_0 is the atmospheric pressure of the trapped air into the cavities, $\theta_y = 36.8°$,[75] and $\varphi = \pi/2 - \theta_s$ with θ_s being the local inclination angle of the surface feature. Since $\tan(\theta_s) \approx \sigma/\xi$, which is also comparable to the slenderness ratio in former studies,[66] we obtained $\varphi \approx \pi/2 - \tan^{-1}(\sigma/\xi)$. Moreover, $R_0 \approx \xi/2$ is the half width of two adjacent features, and $h \approx \sigma$ is a measure of the feature height (the inset of Fig. 7).

Furthermore, we estimated the energy of the system by considering an array of cones of size ξ to represent the surface peaks due to the roughness.[68] The surface area of a cone with the base radius x and height Δh is given by $A_c = \pi x(\Delta h^2 + x^2)^{1/2}$. The latter after substitution yields the more convenient expression $A_c = \pi x^2(1 + \tan\theta_s{}^2)^{1/2}$. Therefore, the energy of the system per unit cell, assuming a checkboard with dimension ξ representing the surface peaks, is given by the relation

$$\begin{aligned} E &= \gamma(\xi^2 - \pi x^2) + (\gamma_{sl} - \gamma_{sv})(A_c) \\ &= \gamma\xi^2 - \gamma\pi x^2[1 + \cos\theta_Y(1 + \tan\theta_s{}^2)^{1/2}], \end{aligned} \quad (4)$$

since $\cos(\theta_y) = (\gamma_{sv} - \gamma_{sl})/\gamma_{lv}$. As x approaches ξ, Eq. (4) shows that the water penetrates deeper into the hydrophilic surface cavities because $\cos\theta_Y > 0$ (since $\theta_Y < 90°$ for hydrophilic surfaces). As a result, the system energy E only decreases with x indicating the absence of a barrier for the transition between the CB and W states. The latter favors the formation of the lower energy W state.

Figure 9 shows calculations of ΔP and E vs the deposition time, from where it becomes clear that the surface cavities lead to large Laplace pressures ΔP ($\gg P_g$). The latter increases with increasing local surface slope σ/ξ (becoming less negative) with the pressure of the liquid P approaching that of the trapped air P_0 in the surface cavity. Therefore, during the first stages of the Cu deposition, the liquid pressure is significantly lower than the cavity pressure prohibiting the wetting of the cavities with the

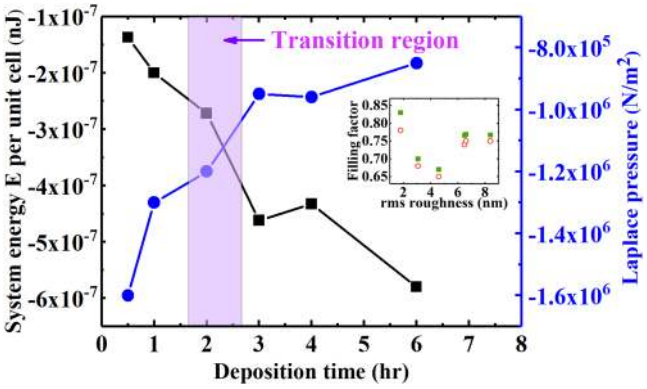

FIG. 9. The variation of the Laplace pressure [Eq. (3)] and the energy E per unit cell [Eq. (4)] with the deposition time for the different Cu surfaces. The inset shows the variation of the Cassie-Baxter filling factor f with the deposition time [open circles, Eq. (5); solid squares, Eq. (6)].

system remaining in a CB-type wetting state. Although ΔP remains negative (e.g., $\Delta P - 8 \times 10^5$ Pa for the roughest film) indicating a convex profile water meniscus in the surface cavities (see the inset of Fig. 7), if the local surface slope is low ($\sigma/\xi \leq 0.2$ for the roughest film, the inset of Fig. 3) then the droplet can spontaneously fill the cavities beneath it. Indeed, the energy of the system E decreases monotonically with surface roughening, indicating that the W state is energetically more favorable for the range of roughnesses that we have here, and the droplet as a whole tends to be in a metastable CB state.

Furthermore, in order to discuss the behavior of contact angle, especially the part of the CB-W transition, we performed some calculations to observe the variation of the filling factor f of the CB state with respect to different surface roughness. In general, a rough surface can be considered as a combination of circular and radial grooves, and the apparent CA θ_{app} on the surface can be defined as the geometric average[76]

$$\frac{2}{\theta_{app}^2} = \frac{1}{\theta_w^2} + \frac{1}{\theta_{CB}^2}. \quad (5)$$

The CA of a smooth Cu surface was measured to be $\theta_y = 36.8°$. The W roughness factor was obtained from the AFM images, and θ_w was given by the Wenzel equation $\theta_w = \cos^{-1}\{r\cos(\theta)\}$. The measurements of θ_{app} from experiment and substitution into Eq. (5) yielded the different θ_{CB} for the different films. Finally, from the Cassie-Baxter equation $\theta_{CB} = \cos^{-1}\{f\cos(\theta) - (1 - f)\}$, we calculated the filling factors f for the different surface roughnesses. As indicated in the inset of Fig. 9, for sample S1, the estimated value for f is $f = 0.78$, and it decreases with increasing roughness to the value $f = 0.65$ for sample S3. After this point, the CB-W transition takes place, indicating the dominance of the W state. For sample S4, for which the wetting transition already occurred, the filling factor has been increased to the value $f = 0.74$ indicating again increased surface wettability. Finally, the values of the filling factor obtained for the rougher samples (S5 and S6) were $f = 0.75$. In addition, we considered the combination of the W and the CB equations to the more general equation[77]

$$\cos(\theta_{app}) = rf\cos(\theta) - (1 - f), \quad (6)$$

from which we obtained comparable filling factors f with those from Eq. (5), as it is shown in the inset of Fig. 9. The relatively low measured apparent CAs (<90°) on the as-deposited surfaces are also reflected by the high calculated filling factors. It should be noted that no meaningful difference is seen in the behaviors of the Laplace pressure, the energy of the system per unit cell, and the filling factor if we consider $\theta_y = 52°$[78] (see the supplementary material, Fig. S1).

V. CONCLUSIONS

In conclusion, we investigated here the static and the dynamic wetting behaviors of copper thin films with controlled growing roughness. The time-dependent height-height correlation functions of the film surfaces indicated anomalous kinetic roughening during the growth with large roughness exponents $\alpha \approx 0.9$, and evolving roughness parameters σ and ξ yielding a nonstationary local surface slope $\rho \approx \alpha/\xi$ that has a strong impact on the surface wettability. In fact, the static and the dynamic CAs revealed two wetting regimes associated with different growth stages leading to the transition from a metastable Cassie-Baxter to a Wenzel state for the roughest films. Increasing surface roughness with uniformly distributed peaks-valleys leads to an increment of the CAs due to the trapped air in surface cavities, while after some point larger surface features lead to lower CAs that varied slightly with further surface roughening. Although the apparent wetting transition with increasing surface roughness is not favored by the local Laplace pressure estimation, since it indicates higher air pressure in surface cavities, the energy of the system decreases with surface roughening, or equivalently increasing local surface slope $\sim\alpha/\xi$, indicating that the Wenzel state is energetically more favorable. Under these conditions, the water droplet can spontaneously fill the surface cavities once the impregnation is initiated by the hydrophilic nature of the surface. This is in agreement with our experiments for significantly large local surface slopes ρ (>0.1) and large roughness exponents $\alpha \sim 1$. Our results indicate that random surface roughening has a complex effect on the wetting properties of surfaces via the local surface slope, and consequently, detailed morphology studies are required to control the impact of rough surfaces on wetting phenomena.

SUPPLEMENTARY MATERIAL

See the supplementary material for similar calculations as those in Fig. 9 but for a different value of the Young contact angle of copper.

ACKNOWLEDGMENTS

F.F. and M.R.M. acknowledge the financial support from the Research Council of the University of Tehran, Iran. G.P. acknowledges support from the Zernike Institute of Advanced Materials, University of Groningen, The Netherlands.

REFERENCES

[1]S. Farhadi, M. Farzaneh, and S. A. Kulinich, Appl. Surf. Sci. **257**, 6264 (2011).

[2]T. T. Isimjan, T. Wang, and S. Rohani, Chem. Eng. J. **210**, 182 (2012).
[3]E. Aljallis, M. A. Sarshar, R. Datla, V. Sikka, A. Jones, and C.-H. Choi, Phys. Fluids **25**, 025103 (2013).
[4]R. Truesdell, A. Mammoli, P. Vorobieff, F. van Swol, and C. J. Brinker, Phys. Rev. Lett. **97**, 044504 (2006).
[5]M. Callies and D. Quéré, Soft Matter **1**, 55 (2005).
[6]H. Yan, H. Shiga, E. Ito, T. Nakagaki, S. Takagi, T. Ueda, and K. Tsujii, Colloids Surf. Physicochem. Eng. Asp. **284–285**, 490 (2006).
[7]Y. Ikada, Biomaterials **15**, 725 (1994).
[8]R. A. Gittens, L. Scheideler, F. Rupp, S. L. Hyzy, J. Geis-Gerstorfer, Z. Schwartz, and B. D. Boyan, Acta Biomater. **10**, 2907 (2014).
[9]T. Young, Phil. Trans. R. Soc. Lond. **95**, 65 (1805).
[10]R. N. Wenzel, Ind. Eng. Chem. **28**, 988 (1936).
[11]A. B. D. Cassie and S. Baxter, Trans. Faraday Soc. **40**, 546 (1944).
[12]D. Quéré, Nat. Mater. **1**, 14 (2002).
[13]D. Quéré, Annu. Rev. Mater. Res. **38**, 71 (2008).
[14]T. Sun, L. Feng, X. Gao, and L. Jiang, Acc. Chem. Res. **38**, 644 (2005).
[15]X. Zhang, F. Shi, J. Niu, Y. Jiang, and Z. Wang, J. Mater. Chem. **18**, 621 (2008).
[16]H. J. Lee and S. Michielsen, J. Text. Inst. **97**, 455 (2006).
[17]G. D. Bixler and B. Bhushan, Soft Matter **8**, 11271 (2012).
[18]R. Fürstner, W. Barthlott, C. Neinhuis, and P. Walzel, Langmuir **21**, 956 (2005).
[19]K. Liu and L. Jiang, Annu. Rev. Mater. Res. **42**, 231 (2012).
[20]Z. Cheng, M. Du, H. Lai, N. Zhang, and K. Sun, Nanoscale **5**, 2776 (2013).
[21]D. Ebert and B. Bhushan, J. Colloid Interface Sci. **384**, 182 (2012).
[22]E. Bormashenko, T. Stein, R. Pogreb, and D. Aurbach, J. Phys. Chem. C **113**, 5568 (2009).
[23]R. Wang, K. Hashimoto, A. Fujishima, M. Chikuni, E. Kojima, A. Kitamura, M. Shimohigoshi, and T. Watanabe, Nature **388**, 431 (1997).
[24]M. Shibuya and M. Miyauchi, Adv. Mater. **21**, 1373 (2009).
[25]D. Lee, M. F. Rubner, and R. E. Cohen, Nano Lett. **6**, 2305 (2006).
[26]M. Chekini, M. R. Mohammadizadeh, and S. M. Vaez Allaei, Appl. Surf. Sci. **257**, 7179 (2011).
[27]A. Ranella, M. Barberoglou, S. Bakogianni, C. Fotakis, and E. Stratakis, Acta Biomater. **6**, 2711 (2010).
[28]P. Bizi-Bandoki, S. Benayoun, S. Valette, B. Beaugiraud, and E. Audouard, Appl. Surf. Sci. **257**, 5213 (2011).
[29]N. Savva, S. Kalliadasis, and G. A. Pavliotis, Phys. Rev. Lett. **104**, 084501 (2010).
[30]C. Huh and S. G. Mason, J. Colloid Interface Sci. **60**, 11 (1977).
[31]T. Onda, S. Shibuichi, N. Satoh, and K. Tsujii, Langmuir **12**, 2125 (1996).
[32]W. Fang, H. Mayama, and K. Tsujii, J. Phys. Chem. B **111**, 564 (2007).
[33]N. J. Shirtcliffe, G. McHale, M. I. Newton, G. Chabrol, and C. C. Perry, Adv. Mater. **16**, 1929 (2004).
[34]Y. Su, B. Ji, K. Zhang, H. Gao, Y. Huang, and K. Hwang, Langmuir **26**, 4984 (2010).
[35]P. Salehikahrizsangi, K. Raeissi, F. Karimzadeh, L. Calabrese, and E. Proverbio, Surf. Coat. Technol. **344**, 626 (2018).
[36]P. K. Dhillon, P. S. Brown, C. D. Bain, J. P. S. Badyal, and S. Sarkar, Appl. Surf. Sci. **317**, 1068 (2014).
[37]G. Palasantzas and J. T. M. de Hosson, Acta Mater. **49**, 3533 (2001).
[38]F. Bottiglione and G. Carbone, Langmuir **29**, 599 (2013).
[39]R. David and A. W. Neumann, J. Phys. Chem. C **116**, 16601 (2012).
[40]C. Yang, U. Tartaglino, and B. N. J. Persson, Phys. Rev. Lett. **97**, 116103 (2006).
[41]B. Shi and V. K. Dhir, J. Chem. Phys. **130**, 034705 (2009).
[42]R. P. Yadav, T. Kumar, V. Baranwal, Vandana, M. Kumar, P. K. Priya, S. N. Pandey, and A. K. Mittal, J. Appl. Phys. **121**, 055301 (2017).
[43]S. Sarkar, S. Patra, N. Gayathri, and S. Banerjee, Appl. Phys. Lett. **96**, 063112 (2010).
[44]S. Patra, S. Sarkar, S. K. Bera, G. K. Paul, and R. Ghosh, J. Appl. Phys. **108**, 083507 (2010).
[45]S. Chatterjee, M. Kumar, S. Gohil, and T. Som, Thin Solid Films **568**, 81 (2014).
[46]X.-F. Tang, Z.-G. Yang, and W.-J. Wang, Colloids Surf. Physicochem. Eng. Asp. **360**, 99 (2010).
[47]J. A. Christians, R. C. M. Fung, and P. V. Kamat, J. Am. Chem. Soc. **136**, 758 (2014).
[48]S. P. Murarka, Mater. Sci. Eng. R Rep. **19**, 87 (1997).
[49]R. Wen, Q. Li, J. Wu, G. Wu, W. Wang, Y. Chen, X. Ma, D. Zhao, and R. Yang, Nano Energy **33**, 177 (2017).
[50]G. H. ten Brink, G. Krishnan, B. J. Kooi, and G. Palasantzas, J. Appl. Phys. **116**, 104302 (2014).
[51]G. Palasantzas and J. Krim, Phys. Rev. B **48**, 2873 (1993).
[52]G. Palasantzas and J. Krim, Phys. Rev. Lett. **73**, 3564 (1994).
[53]G. Palasantzas, Phys. Rev. E **56**, 1254 (1997).
[54]J. M. López, M. A. Rodríguez, and R. Cuerno, Physica A **246**, 329 (1997).
[55]Y.-P. Zhao, *Characterization of Amorphous and Crystalline Rough Surface: Principles and Applications* (Elsevier, San Diego, CA, 2000).
[56]M. A. Auger, L. Vázquez, R. Cuerno, M. Castro, M. Jergel, and O. Sánchez, Phys. Rev. B **73**, 045436 (2006).
[57]J. H. Jeffries, J.-K. Zuo, and M. M. Craig, Phys. Rev. Lett. **76**, 4931 (1996).
[58]T. Karabacak, Y.-P. Zhao, G.-C. Wang, and T.-M. Lu, Phys. Rev. B **64**, 085323 (2001).
[59]Z. Li, Y. Wang, A. Kozbial, G. Shenoy, F. Zhou, R. McGinley, P. Ireland, B. Morganstein, A. Kunkel, S. P. Surwade, L. Li, and H. Liu, Nat. Mater. **12**, 925 (2013).
[60]M. K. Bernett and W. A. Zisman, J. Phys. Chem. **74**, 2309 (1970).
[61]T. Zubkov, D. Stahl, T. L. Thompson, D. Panayotov, O. Diwald, and J. T. Yates, J. Phys. Chem. B **109**, 15454 (2005).
[62]L. B. Boinovich, A. M. Emelyanenko, A. S. Pashinin, C. H. Lee, J. Drelich, and Y. K. Yap, Langmuir **28**, 1206 (2012).
[63]A. Borras and A. R. González-Elipe, Langmuir **26**, 15875 (2010).
[64]E. J. Lobaton and T. R. Salamon, J. Colloid Interface Sci. **314**, 184 (2007).
[65]D. Murakami, H. Jinnai, and A. Takahara, Langmuir **30**, 2061 (2014).
[66]Q.-S. Zheng, Y. Yu, and Z.-H. Zhao, Langmuir **21**, 12207 (2005).
[67]P. Papadopoulos, L. Mammen, X. Deng, D. Vollmer, and H.-J. Butt, Proc. Natl. Acad. Sci. U.S.A. **110**, 3254 (2013).
[68]P. Li, J. Xie, and Z. Deng, Appl. Surf. Sci. **335**, 29 (2015).
[69]R. David and A. W. Neumann, Colloids Surf. Physicochem. Eng. Asp. **425**, 51 (2013).
[70]B. He, N. A. Patankar, and J. Lee, Langmuir **19**, 4999 (2003).
[71]P. Tsai, R. G. H. Lammertink, M. Wessling, and D. Lohse, Phys. Rev. Lett. **104**, 116102 (2010).
[72]N. R. Pallas and Y. Harrison, Colloids Surf. **43**, 169 (1990).
[73]P.-G. de Gennes, F. Brochard-Wyart, and D. Quéré, in *Capillarity Wetting Phenomena. Drops, Bubbles, Pearls, Waves*, edited by P.-G. de Gennes, F. Brochard-Wyart, and D. Quéré (Springer, New York, NY, 2004), pp. 33–67.
[74]Y. Tsori, Langmuir **22**, 8860 (2006).
[75]T. de Wolf, "Contact angles of various liquids on silicon/copper with copper nanoparticles," Master thesis (University of Groningen, 2017).
[76]X. B. Zhou and J. T. M. D. Hosson, J. Mater. Res. **10**, 1984 (1995).
[77]A. Marmur, Langmuir **19**, 8343 (2003).
[78]M. Yekta-fard and A. B. Ponter, J. Adhes. **18**, 197 (1985).